Wiley
International Journal of Energy Research
Volume 2024, Article ID 5627453, 15 pages
https://doi.org/10.1155/2024/5627453

WILEY

Research Article

Bayesian Optimization of Operating Points of a Continuous Perhydro-Dibenzyltoluene Dehydrogenation Reactor

Alexander Verhoolen[1], **Michael Geißelbrecht**[2], **Julian Kadar**[2], **Patrick Preuster**[3,4], **Peter Wasserscheid**[2,5] and **Knut Graichen**[1]

[1]*Chair of Automatic Control, Friedrich-Alexander-Universität Erlangen-Nürnberg, Cauerstr. 7, Erlangen 91058, Germany*
[2]*Helmholtz-Institute Erlangen-Nürnberg for Renewable Energy (IET-2), Forschungszentrum Jülich, Egerlandstr. 3, Erlangen 91058, Germany*
[3]*Rosenheim Technical University of Applied Sciences, Robert-Koch-Straße 28, Burghausen 84489, Germany*
[4]*Fraunhofer IEG, Fraunhofer Research Institution of Energy Infrastructure and Geothermal Systems IEG, Am Hochschulcampus 1, Bochum 44801, Germany*
[5]*Institute of Chemical Reaction Engineering, Friedrich-Alexander-Universität Erlangen-Nürnberg, Egerlandstr. 3, Erlangen 91058, Germany*

Correspondence should be addressed to Alexander Verhoolen; alexander.verhoolen@fau.de

Received 18 September 2023; Revised 27 June 2024; Accepted 13 September 2024

Academic Editor: Zhien Zhang

Liquid organic hydrogen carriers (LOHCs) are a promising option for hydrogen storage, but a high efficiency of the LOHC cycle is essential in order to serve as an attractive technology in the context of decarbonization. This paper presents different methods to optimize steady-state operating points of a LOHC dehydrogenation (DH) reactor. For this purpose, an analytical model of a DH reactor is described, which is extended to a hybrid model (HM) to achieve sufficient model accuracy. The model quality is subsequently validated by measurements. For the optimization of the steady-state operation point, a Bayesian optimization framework is presented and compared to classical model-based optimization. The methods are evaluated with the HM as well as with experimental results.

Keywords: Bayesian optimization; dehydrogenation; hydrogen storage; LOHC; operating point optimization

1. Introduction

In recent times, a transition to renewable energies has taken place in all energy sectors. Hydrogen plays a significant role as an energy carrier, not only as a substitute for fossil fuels [1]. It has already been shown in several studies that the storage and transport of hydrogen via liquid organic hydrogen carriers (LOHCs) offers several advantages over conventional storage technologies like cryogenic or compressed hydrogen [1, 2].

LOHC systems are composed of pairs of hydrogen-lean, typically aromatic, and hydrogen-rich, typically alicyclic, compounds. In their basic form, LOHCs are usually present in a hydrogen-lean form (H0-LOHC). The storage of hydrogen occurs through exothermic hydrogenation of the aromatic compounds, leading to the LOHC system in its hydrogen-rich form (Hx-LOHC). The Hx-LOHC can be transported and stored similar to liquid fossil fuels [3]. The release of hydrogen from Hx-LOHC is realized by an endothermic dehydrogenation (DH) that converts the hydrogen-rich Hx-LOHC to its hydrogen-lean H0-LOHC form. As an example, the chemical hydrogen storage cycle is illustrated in Figure 1 for the example of the LOHC system dibenzyltoluene (DBT) (H0-DBT)/perhydro-dibenzyltoluene (H18-DBT) as it is used in the following of this paper.

Over the last years, various substances have been investigated for their suitability as LOHC, such as methylcyclohexane (MCH) or N-ethyl carbazole (NEC). An overview of common LOHC systems and their properties is given by

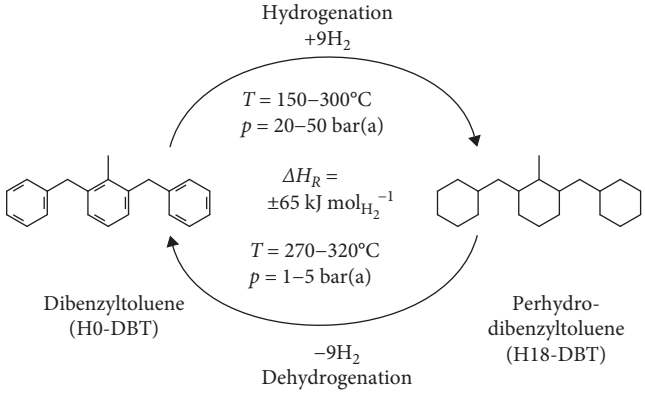

FIGURE 1: Schematic diagram of hydrogenation/dehydrogenation of dibenzyltoluene (H0-DBT)/perhydro-dibenzyltoluene (H18-DBT) LOHC system [4]. LOHC, liquid organic hydrogen carrier.

Aakko-Saksa et al. [2] and Rao and Yoon [3]. Brückner et al. [5] presented the promising LOHC system of dibenzyltoluene (H0-DBT) and perhydro-dibenzyltoluene (H18-DBT), which is used in this paper. H0-DBT is an industrially well-established heat transfer oil, for example, under the brand Marlotherm SH. The thermophysical and thermochemical properties of the DBT system were studied by Müller et al. [6]. Jorschick et al. [7] showed the stability of this LOHC system over numerous charging/discharging cycles.

Particularly in the field of DH of H18-DBT, different catalysts and reactor setups have been investigated to improve the overall efficiency. Fikrt et al. [8] studied the DH of H18-DBT in a horizontal fixed-bed tubular reactor. They focused on the dynamics of DH induced by changes in LOHC feed flow rate, reactor temperature, and reactor pressure. In further studies, different kinetic models for the DH of H18-DBT with different catalysts were presented [9, 10]. Thereby it is shown that the complex reaction network with multiple isomers of H18-DBT, H12-DBT, H6-DBT, and H0-DBT can be simplified considering only direct DH from H18-DBT to H0-DBT. The concentration of H18-DBT represents an effective concentration for the amount of reversible bound hydrogen. The studies were investigated in both plug-flow reactors and batch reactors. The first cuboid flow reactor for DH of H18-DBT was considered in a study of coupling the reactor with a solid oxide fuel cell to increase efficiency from LOHC-bound hydrogen to electricity [11]. The cuboid flow reactor concept was further refined in Geißelbrecht et al. [12], where a gas pathway was added for passing the hydrogen along the catalyst. In addition, a model for hydrogen release considering the evaporation of H0-DBT and H18-DBT was described in [12]. In Bollmann et al. [13], a novel concept for heat input into a DH reactor is presented. Thereby, the reaction volume is crossed by a large number of tubes through which hot gas is passed, and thus a uniform heat input is achieved. Other interesting reactor concepts are the hot pressure swing reactor [7], in which hydrogenation and DH take place in the same reactor, a multistage membrane plug flow reactor, in which the released hydrogen is separated from the gas phase by a membrane [14], and the DehyMax reactor, which uses the concept of an inverted multitubular reactor with crossflow heating [15].

The above discussion shows that previous research in the field of DH has focused primarily on improving the catalyst and reactor development. In the present paper, the control variables of the DH reactor consisting of the LOHC feed flow rate, reactor temperature, and reactor pressure are used to optimize the stationary operating points of the reactor with respect to predefined goals.

Classical numerical optimization methods can be distinguished in unconstrained and constrained optimization. Unconstrained optimization is the minimization of a function over specific optimization variables and typically relies on line search or trust region methods. Meanwhile, constrained optimization additionally considers (nonlinear) equality or inequality constraints as a function of the optimization variables. Popular methods are sequential quadratic programing (SQP) or interior point (IP) methods [16, 17]. These algorithms rely on gradient or even Hessian information. However, in process control and, in particular, in case of the LOHC DH reactor considered in this paper, process evaluations and, thus, data generation are very expensive. On the other hand, analytical modeling based on physical equations (white box model) is generally limited in accuracy for complex processes, as simplification often has to be made in the model design due to a lack of process knowledge.

An alternative approach is pure data-based modeling (black box model), which requires a large amount of data for training in order to obtain sufficient accuracy. For this reason, chemical processes are often described using hybrid models (HMs) [18]. Sohlberg and Jacobsen [19] described different structures of HMs. These include both a white box model, which represents available process knowledge, and a black box model, which describes unknown mechanisms. For the black box model, different machine learning methods can be used. For example, Molga [20] used artificial neural networks (ANNs) for modeling chemical reactors. Zhang et al. [21] presented a HM using Gaussian process regression (GPR) to describe chemical reactors in water treatment. Shokry et al. [22] modeled a batch process using ordinary kringing (OK), ANN, and GPR and compared the methods afterward.

Model-free optimization stands in contrast to classical numerical optimization, which uses one of the abovementioned types of models. A popular method in this context is Bayesian optimization (BO), for which no model of the process to be optimized is necessary. This renders BO especially favorable for the optimization of complex processes. To this end, a surrogate model iteratively learns the function to be optimized. The points at which the target function is evaluated are determined by the optimization of an acquisition function. BO is described by Brochu, Cora, and De Freitas [23] in detail. The use of a surrogate model is a very efficient approach to keep the number of expensive process evaluations low [24–27]. Especially due to this advantage over conventional optimization algorithms, BO has already found application in various areas of chemistry [28–30]. In Stecher, Kiltz, and Graichen [31], a BO-based approach for robust design optimization of a batch reactor is presented.

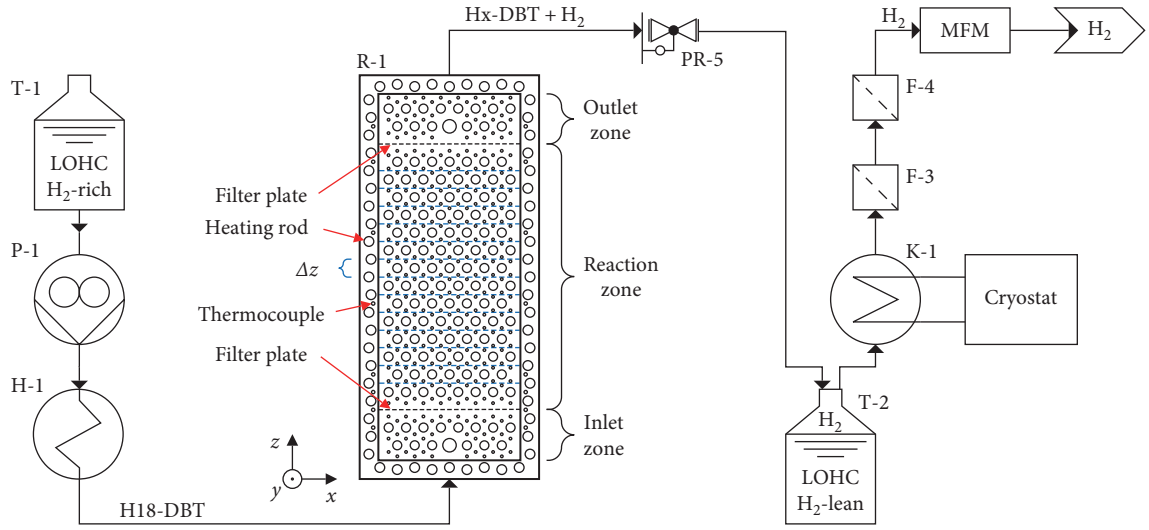

FIGURE 2: Experimental LOHC dehydrogenation plant with cuboid dehydrogenation reactor [15]. DBT, dibenzyltoluene; LOHC, liquid organic hydrogen carrier, MFM, mass flow meter.

In this paper, three methods for optimizing the operating points of LOHC DH reactors are presented and compared. The aim is to find the most efficient control variables, consisting of LOHC volume flow rate, reactor temperature, and reactor pressure, for a required hydrogen volume flow rate that is required, for example, by downstream apparatuses. Previous studies have mainly focused on optimizing the chemical process itself rather than the efficient operating points. For this purpose, a model-based BO is applied in addition to the conventional approach of model-based nonlinear optimization (NO). A HM of the process is developed and used for both model-based methods. In comparison to the two previously mentioned methods, a model-free BO is applied as a third approach, which is applied directly to a real process and therefore no complex modeling is necessary.

The paper is outlined as follows: The considered continuous cuboid DH reactor is described in Section 2. In Section 3, a steady-state HM of the considered reactor is presented, which is used for the subsequent optimization. A validation of the HM is given in Section 4. The optimization of the operating points with the corresponding optimization problem and the BO as an alternative approach to classical numerical optimization is presented in Section 5. Subsequently, an evaluation and comparison of the three applied optimization procedures are given in Section 6, before conclusions are drawn in Section 7.

2. Continuous Cuboid Dehydrogenation Reactor

This paper considers a continuous cuboid DH reactor as part of an experimental DH plant. Figure 2 shows a simplified flow sheet of the plant and a schematic representation of the reactor that uses dibenzyltoluene (H0-DBT)/perhydro-dibenzyltoluene (H18-DBT) as LOHC system [15]. The hydrogen-rich H18-DBT is fed from the reactant tank into the reactor by a magnet membrane dosing pump, at which the LOHC volume flow rate can be adjusted. The volume flow passes through a preheater where it is heated to a desired temperature. Subsequently, the H18-DBT flows upward (in z-direction) through the vertically mounted reactor.

The reactor is made of stainless steel and has a length of 164 mm, width of 120 mm, and height of 364 mm. It is divided into three zones, the inlet zone, the reaction zone, and the outlet zone. The different zones are separated by filter plates, which ensure a homogeneous flow at the beginning of the reaction zone. In addition, the filter plates fix the catalyst in the reaction zone. The catalyst used is 0.3 wt% Pt/Al_2O_3 with a mean pellet diameter of 2.6 mm. In total, the reactor is filled with 1.4 kg catalyst pellets. The energy required by the endothermic DH reaction is provided by heating rods (HRs). A total of 151 HRs and 118 thermocouples (TCs) are installed in the reactor, which are distributed inside over all zones as well as mounted in the frame. A desired reactor temperature can be adjusted by a temperature controller. By using multiple heating zones over the length of the reactor, an approximately homogeneous temperature distribution can be achieved in the reactor. In addition, the entire reactor is insulated to minimize heat loss.

The reactor is designed for a pressure of up to 8 bar(a) and a temperature up to 400°C in the HRs. A pressure between 2 and 4 bar(a) and a LOHC flow rate between 1 and 3 $L\,h^{-1}$ were chosen as standard reaction conditions. The HRs were controlled to obtain a catalyst temperature between 280 and 320°C [15]. Measurements have shown that there is a negligible pressure drop over the reaction zone, which is less than 0.01 bar(a).

The preheated H18-DBT flows into the inlet zone, where it is heated to the desired reactor temperature. Subsequently, the liquid flows further into the reaction zone where the endothermic DH reaction takes place and hydrogen is released. Furthermore, DBT with a certain hydrogen content (Hx-DBT) evaporates and a mixture of gaseous released hydrogen, evaporated and liquid Hx-DBT is formed. Finally, the resulting two-phase mixture flows through the outlet zone before exiting the reactor at the top.

A pressure retention valve is mounted after the reactor, which enables the reactor pressure to be controlled. The mixture then flows into the product tank, where the liquid and condensed hydrogen-lean Hx-DBT are separated from the hydrogen stream. The hydrogen stream further flows through a partial condenser, resulting in cooling of the gas stream and complete separation of the hydrogen from the Hx-DBT. Subsequently, the hydrogen stream passes two active carbon filters, which remove the light boiling decomposition products, before finally the hydrogen volume flow is measured by a digital mass flow meter (MFM).

The hydrogen volume flow rate at the reactor exit depends on three control variables consisting of the LOHC feed flow $\dot{V}_{\mathrm{LOHC,in}}$, the reactor temperature T, and the reactor pressure p. The control variables are combined in the input vector

$$\boldsymbol{z} = \begin{bmatrix} \dot{V}_{\mathrm{LOHC,in}} \\ T \\ p \end{bmatrix} \in [\boldsymbol{z}^{-}, \boldsymbol{z}^{+}], \tag{1}$$

subject to physical box constraints with

$$\boldsymbol{z}^{-} = \begin{bmatrix} 1\,\mathrm{L\,h^{-1}} \\ 280\,^{\circ}\mathrm{C} \\ 2\,\mathrm{bar(a)} \end{bmatrix}, \; \boldsymbol{z}^{+} = \begin{bmatrix} 3\,\mathrm{L\,h^{-1}} \\ 320\,^{\circ}\mathrm{C} \\ 4\,\mathrm{bar(a)} \end{bmatrix}. \tag{2}$$

3. Model of Released Hydrogen Flow

This section presents a model for the released hydrogen volume flow $\dot{V}_{\mathrm{H_2}}$ as a function of the input variables (Equation 1). For this purpose, an analytical model (AM) is derived using the mass balance of the reactor and considering the evaporation of the LOHC, before the focus is put on steady-state operating points. In the second step, the AM is extended to a HM using GPR to account for the uncertainties of the process that are not captured by the physical model.

3.1. Mass Balance of Cuboid Dehydrogenation Reactor. The release of hydrogen is described by the mass balance of the reactor. In general, the mass balance equation for a chemical species i in a reactor with flowing fluid of varying temperature, density, and composition is defined as

$$\frac{\partial c_i}{\partial t} = -\nabla \cdot (c_i \boldsymbol{u}) - \nabla \cdot (\boldsymbol{D}_{\mathrm{e}} \nabla c_i) + r_i, \tag{3}$$

where $c_i(t, x, y, z)$ is the concentration of species i depending on time t and the spatial position (x, y, z), $\boldsymbol{u}(t, x, y, z)$ is the velocity vector of the fluid, $\boldsymbol{D}_{\mathrm{e}}(x, y, z)$ is the effective dispersion coefficient, and r_i is the total rate of change of the amount of component i. The operator ∇f represents the gradient of a scalar function f and $\nabla \cdot g$ the divergence of a vector function g [32, 33].

The expression in Equation (3) can be divided into four terms: The term on the left side is the accumulation term. This indicates the change in the amount of substance of species i over time. In the case of the cuboid flow reactor presented in Section 2, a simplified reaction for the DH is assumed, as shown in Figure 1. Thereby, the intermediates H6-DBT and H12-DBT, formed during the reaction from H18-DBT to H0-DBT, are neglected. With this simplification, the DH reaction can be described sufficiently accurately [12]. Consequently, the mass balance includes the liquid phase, consisting of H0-DBT and H18-DBT, and the gas phase, consisting of the released hydrogen.

The first term on the right side of Equation (3) is the convection term. Considering the presented cuboid flow reactor, it is observed that the flow in z-direction is predominant. Therefore, the convection term is simplified by neglecting the fluid velocities in other directions. Furthermore, the minor change in the density of the DBT during the reaction from H18-DBT to H0-DBT is neglected. Hence, the volume flow rate $\dot{V}_{\mathrm{L}}$ of the liquid phase and consequently the flow velocity u_{L} of the liquid phase in z-direction can be assumed to be constant. The material properties of H0-DBT and H18-DBT are presented in Müller et al. [6]. The gas phase velocity can be determined based on the total gaseous volume flow $\dot{V}_{\mathrm{G}}$ and the available cross-section A_{G} for the gas flow. Thus, the flow velocities u_{L} and u_{G} of the two phases in z-direction can be described by

$$u_L = \frac{\dot{V}_{\mathrm{L}}}{A_{\mathrm{L}}} = \frac{\dot{V}_{\mathrm{L}}}{A_{\mathrm{R}} H_{\mathrm{L}}}, \tag{4a}$$

$$u_G = \frac{\dot{V}_{\mathrm{G}}}{A_{\mathrm{G}}} = \frac{\dot{V}_{\mathrm{G}}}{A_{\mathrm{R}}(1 - H_{\mathrm{L}})}, \tag{4b}$$

where A_{R} is the total cross-sectional area of the reactor. The liquid holdup H_{L} indicates the fraction of the liquid phase in the total. It can be calculated according to Stiegel and Shah [34] by

$$H_{\mathrm{L}} = \overline{\alpha} Re_{\mathrm{L}}^{\overline{\beta}} Re_{\mathrm{G}}^{\overline{\gamma}} (a_{\mathrm{s}} d_{\mathrm{s}})^{\overline{\delta}}, \tag{5}$$

where Re_{L} and Re_{G} are the Reynolds numbers of the liquid phase and gas phase, a_{s} is the external surface area per unit volume of particle, and d_{s} is the equivalent packing diameter. The constants $\overline{\alpha}$, $\overline{\beta}$, $\overline{\gamma}$, and $\overline{\delta}$ are adjustable parameters. The liquid holdup H_{L} changes over the reactor height as the Reynolds number of the gas phase changes with the reactor height considering the influence of the formed hydrogen on the complex hydrodynamics. The holdup decreases with increasing amount of formed hydrogen. Furthermore, it is assumed that an ideal homogenization prevails in xy-plane. Hence, the concentration of species i results in

$$c_i(t, x, y, z) = c_i(t, z). \tag{6}$$

The second term in Equation (3) is the dispersion term, which specifies the change in the amount of substance of

species i over time caused by dispersion. In this case, an ideal plug flow behavior is assumed and so the dispersion term can be neglected.

The last term in Equation (3) is the total rate r_i of change in the amount of component i caused by chemical reactions. It is composed of the partial reactions in the reaction system. As already mentioned, the reaction from H18-DBT to H0-DBT can be described in a sufficiently accurate simplified way by

$$\text{H18-DBT} \rightleftarrows \text{H0-DBT} + 9\text{H}_2, \tag{7}$$

where H18-DBT reacts in a reversible reaction with the release of $9H_2$ to H0-DBT. In this case, the total reaction rate r can be described by the reaction from H18-DBT to H0-DBT and its reverse reaction by

$$r = k_0 C \exp\left(-\frac{E_A}{RT}\right) c_{\text{H18-DBT}} - \frac{k_0}{K_{eq}} C \exp\left(-\frac{E_A}{RT}\right) c_{\text{H0-DBT}}. \tag{8}$$

Both partial reactions in Equation (8) are described by a power law approach. The rate coefficient k is described by Arrhenius equation [32]. The pre-exponential factor k_0 and the activation energy E_A are determined according to Geißelbrecht et al. [12]. The constant

$$C = \frac{a_{cat} m_{cat} w_{nm}}{V_{LOHC}} \tag{9}$$

represents the properties of the catalyst in the reactor and depends on the catalyst mass m_{cat}, the mass fraction of noble metal in the catalyst w_{nm}, the volume of LOHC in the reactor V_{LOHC}, and a catalyst activity coefficient a_{cat}. Therefore, the reaction rate r can be adjusted to different catalyst conditions. The kinetic approach is only valid for the hydrogen release from liquid H18-DBT and thus we assumed that the hydrogen release is only possible from liquid H18-DBT. Over the catalyst lifetime, the reaction can be inhibited by various effects, as described, for example, in Wunsch, Berg, and Pfeifer [35] or Solymosi et al. [36]. The occurring effects are not sufficiently studied to express them analytically. For this reason, a_{cat} is assumed to be constant and determined from measurement data. The chemical equilibrium between the two partial reactions is expressed by the equilibrium constant K_{eq}. Since the hydrogen produced is gaseous, the DH is a biphasic reaction. Therefore, the equilibrium constant K_{eq} has to be defined by a heterogeneous equilibrium [37]. In Geißelbrecht et al. [12], K_{eq} is derived as

$$K_{eq} = \frac{c_{\text{H0-DBT,eq}}}{c_{\text{H18-DBT,eq}}} = \frac{DoDH_{eq}}{\left(1 - DoDH_{eq}\right)}, \tag{10}$$

not considering the concentration of gaseous hydrogen. The molar concentrations at equilibrium are given by $c_{\text{H0-DBT,eq}}$ and $c_{\text{H18-DBT,eq}}$, and $DoDH_{eq}$ denotes the degree of dehydrogenation (DoDH) at equilibrium. It is defined as the ratio of the amount of released hydrogen to maximum amount of reversibly releasable hydrogen. In Dürr et al. [38], a correlation for $DoDH_{eq}$ as a function of temperature and pressure is described.

With the assumptions described above, the mass balance (Equation 3) for the presented cuboid DH reactor results in

$$\frac{\partial c_{\text{H0-DBT}}}{\partial t} = -u_L \frac{\partial c_{\text{H0-DBT}}}{\partial z} + r, \tag{11a}$$

$$\frac{\partial c_{\text{H18-DBT}}}{\partial t} = -u_L \frac{\partial c_{\text{H18-DBT}}}{\partial z} - r, \tag{11b}$$

$$\frac{\partial c_{\text{H}_2}}{\partial t} = -u_G \frac{\partial c_{\text{H}_2}}{\partial z} + 9r, \tag{11c}$$

$$c_i(0, z) = c_{i,0}, \quad c_i(t, 0) = c_{i,\text{in}}. \tag{11d}$$

Using the mass balance of the cuboid DH reactor shown in Equations (11a)–(11d), the hydrogen volume flow $\dot{V}_{\text{H}_2}$ at normal conditions at the outlet of the reactor can be expressed by

$$\dot{V}_{\text{H}_2} = 9 \frac{\dot{V}_L}{c_{\text{H}_2,N}} c_{\text{H0-DBT}}(t, L_z), \tag{12}$$

where $c_{\text{H}_2,N}$ is the concentration of hydrogen at normal conditions and L_z the length of the reactor in z-direction. It should be emphasized that Equation (11c) is not needed for the calculation of $\dot{V}_{\text{H}_2}$ and therefore the model can be simplified.

3.2. Conversion Model. A further simplifying assumption is that the LOHC feed stream consists entirely of H18-DBT. As a result, the amount of substance $n_{\text{H18-DBT}}$ of H18-DBT can be described as the difference in the amounts of substances $n_{\text{H18-DBT,in}}$ of H18-DBT at the inlet of the reactor and $n_{\text{H0-DBT}}$ of H0-DBT. Under the assumptions of a constant volume of the liquid phase, it follows

$$c_{\text{H18-DBT}} = c_{\text{H18-DBT,in}} - c_{\text{H0-DBT}}. \tag{13}$$

In addition, the conversion

$$X(t, z) = \frac{c_{\text{H0-DBT}}}{c_{\text{H18-DBT,in}}} = 1 - \frac{c_{\text{H18-DBT}}}{c_{\text{H18-DBT,in}}}, \tag{14}$$

is introduced to further simplify the model without loss of information. It indicates the proportion of the substance converted by the chemical reaction in relation to the substance feed [39].

The transformed mass balance system for describing the hydrogen volume flow of the cuboid flow reactor is as follows

$$\frac{\partial X}{\partial t} = -u_{\mathrm{L}} \frac{\partial X}{\partial z} + r_{\mathrm{X}}, \tag{15a}$$

$$\dot{V}_{\mathrm{H_2}} = 9 \frac{c_{\mathrm{H18-DBT,in}}}{c_{\mathrm{H_2,N}}} \dot{V}_{\mathrm{L}} X(t, L_{\mathrm{z}}), \tag{15b}$$

$$X(0, z) = X_0, \quad X(t, 0) = 0, \tag{15c}$$

$$r_{\mathrm{X}} = k_0 C \exp\left(-\frac{E_{\mathrm{A}}}{RT}\right) c_{\mathrm{H18-DBT,in}} \left(1 - \left(1 - \frac{1}{K_{\mathrm{eq}}}\right) X\right). \tag{15d}$$

The released hydrogen flow $\dot{V}_{\mathrm{H_2}}$ is only dependent on the concentration change of H18-DBT. As we assumed only hydrogen release from liquid H18-DBT, the concentration change of H18-DBT and hydrogen is only dependent on the liquid phase velocity u_{L} and the gas phase velocity u_{G} must not be considered.

3.3. Evaporation of LOHC. In the previous section, it is assumed in a simplified way that the liquid holdup H_{L} and therefore also the liquid phase velocity u_{L} are constant. As described in Geißelbrecht et al. [12], evaporation of the LOHC occurs particularly at high reactor temperatures or low reactor pressures. A common approach to describe the mass transfer that occurs between the liquid and gas phases is the two-film theory [32, 40], which assumes that the mass transfer does not occur directly between the liquid phase and the gas phase but through an interface. The mass transfer between the phases and the interface is calculated by the concentration differences or pressure differences and a corresponding mass transfer coefficient. For the presented LOHC system, however, the mass transfer coefficients are not known, which is why an alternative approach based on Geißelbrecht et al. [12] is used here.

It is assumed in the following that the liquid phase and the gas phase are in equilibrium at all times, that is, there is a vapor–liquid equilibrium (VLE). The phase equilibrium is characterized by both phases being in thermodynamic equilibrium and having the same chemical potential. The VLE is described in a simplified way using Rauolt's law, which is based on the fact that the fugacity of the two phases in the VLE is the same. Raoult's law then becomes

$$x_i P_i^{\mathrm{LV}} = y_i p, \tag{16}$$

where x_i is the molar fraction of component i in the liquid phase, y_i is the molar fraction of component i in the gas phase, p is the pressure in the reactor, and P_i^{LV} is the vapor pressure of component i [41]. The vapor pressure of H0-DBT and H18-DBT can be calculated using the correlation in Jorschick et al. [42]. For hydrogen, the fugacity according to Prausnitz and Shair [43] is used instead of the vapor pressure. Table 1 shows the calculated vapor pressures and fugacity for various temperatures in the temperature range of the cuboid reactor. It can be seen that the fugacity of hydrogen is much larger with respect to the vapor pressures. Therefore, it can be assumed in a simplified way that the hydrogen is still present only in the gas phase and thus no solubility of the hydrogen in the liquid phase needs to be considered.

TABLE 1: Vapor pressures of H0-DBT $P^{\mathrm{LV}}_{\mathrm{H0-DBT}}$ and H18-DBT $P^{\mathrm{LV}}_{\mathrm{H18-DBT}}$ calculated with the correlation from [42] and fugacity of hydrogen $P^{\mathrm{LV}}_{\mathrm{H_2}}$ using the correlation from [43] for selected temperature.

T (°C)	$P^{\mathrm{LV}}_{\mathrm{H0-DBT}}$ (Pa)	$P^{\mathrm{LV}}_{\mathrm{H18-DBT}}$ (Pa)	$P^{\mathrm{LV}}_{\mathrm{H_2}}$ (Pa)
280	6.331×10^3	1.064×10^3	1.988×10^7
300	1.146×10^3	1.860×10^3	1.838×10^7
320	1.965×10^3	3.105×10^3	1.704×10^7

Abbreviation: DBT, dibenzyltoluene.

Due to the evaporation of the LOHC, it can no longer be assumed that the volume flow of the liquid phase $\dot{V}_{\mathrm{L}}$ remains constant over the reactor. Thus, the flow velocity of the liquid phase u_{L} is also no longer constant and must be calculated accordingly. This can be expressed by

$$u_L = \frac{\dot{V}_{\mathrm{L}}}{A_{\mathrm{L}}} = \frac{\dot{n}_{\mathrm{L}} M_{\mathrm{L}}}{A_{\mathrm{R}} H_{\mathrm{L}} \rho_{\mathrm{L}}}, \tag{17}$$

where A_{L} is the cross-sectional area of the liquid phase in the reactor, H_{L} is the liquid holdup, A_{R} is the total cross-sectional area of the reactor, and $\dot{n}_{\mathrm{L}}$ is the molar flux of the liquid phase. The molar mass is M_{L} and ρ_{L} denotes the density of the liquid phase. Corresponding values and correlations are presented in Müller et al. [6].

Due to the VLE and the variable liquid holdup, the following algebraic conditions must be fulfilled when solving Equations (15a)–(15d):

$$u_L = \frac{\dot{n}_\mathrm{L} M_\mathrm{L}}{A_\mathrm{R} H_\mathrm{L} \rho_\mathrm{L}}, \tag{18a}$$

$$\frac{p}{P^{\mathrm{LV}}_{\mathrm{H0-DBT}}} = \frac{\dot{n}_{\mathrm{L,H0-DBT}}}{\dot{n}_\mathrm{L}} \frac{\dot{n}_\mathrm{G}}{\dot{n}_{\mathrm{G,H0-DBT}}}, \tag{18b}$$

$$\frac{p}{P^{\mathrm{LV}}_{\mathrm{H18-DBT}}} = \frac{\dot{n}_{\mathrm{L,H18-DBT}}}{\dot{n}_\mathrm{L}} \frac{\dot{n}_\mathrm{G}}{\dot{n}_{\mathrm{G,H18-DBT}}}, \tag{18c}$$

$$X = \frac{\dot{n}_{\mathrm{L,in}} - \dot{n}_{\mathrm{L,H18-DBT}} - \dot{n}_{\mathrm{G,H18-DBT}}}{\dot{n}_{\mathrm{L,in}}}, \tag{18d}$$

$$\dot{n}_\mathrm{L} = \dot{n}_{\mathrm{L,H18-DBT}} + \dot{n}_{\mathrm{L,H0-DBT}}, \tag{18e}$$

$$\dot{n}_G = \dot{n}_{\mathrm{G,H18-DBT}} + \dot{n}_{\mathrm{G,H0-DBT}} + 9\left(\dot{n}_{\mathrm{L,H0-DBT}} + \dot{n}_{\mathrm{G,H0-DBT}}\right), \tag{18f}$$

$$\dot{n}_{\mathrm{L,in}} = \dot{n}_{\mathrm{L,H18-DBT}} + \dot{n}_{\mathrm{L,H0-DBT}} + \dot{n}_{\mathrm{G,H18-DBT}} + \dot{n}_{\mathrm{G,H0-DBT}}, \tag{18g}$$

$$H_\mathrm{L} = \overline{\alpha} Re_\mathrm{L}^{\overline{\beta}} Re_\mathrm{G}^{\overline{\gamma}} (a_\mathrm{s} d_\mathrm{s})^{\overline{\delta}}, \tag{18h}$$

where $\dot{n}_\mathrm{L}$ and $\dot{n}_\mathrm{G}$ are the molar flux of the liquid and gas phase, $\dot{n}_{\mathrm{L,H18-DBT}}$ and $\dot{n}_{\mathrm{G,H18-DBT}}$ are the molar flux of H18-DBT in the liquid and gas phases, $\dot{n}_{\mathrm{L,H0-DBT}}$ and $\dot{n}_{\mathrm{G,H0-DBT}}$ are the molar flux of H0-DBT in the liquid and gas phases, and $\dot{n}_{\mathrm{L,in}}$ is the molar flux of the liquid phase at the inlet of the reactor. This set of equations can be solved algebraically and expressed by the flow velocity $u_L = f(\dot{V}_{\mathrm{L,in}}, T, p, X)$ as a function of the inflow volume flow $\dot{V}_{\mathrm{L,in}}$, the temperature T, the pressure p, and the conversion X.

3.4. Steady-State Model. The optimization of the operating points is based on a steady-state model for the released hydrogen volume flow $\dot{V}_{\mathrm{H_2}}$. In order to obtain the steady-state model, the time derivative on the left-hand side of Equation (15a) is set to zero, which allows the stationary conversion $\overline{X}$ to be expressed by

$$\overline{X}(z) \coloneqq X(t,z) \text{ with } \frac{\partial \mathrm{X}}{\partial \mathrm{t}} = 0. \tag{19}$$

For the calculation of the stationary conversion $\overline{X}$ backward differences of the partial differential Equation (15a) over the position variable z are used. The resulting discretization can also be interpreted as a cascade of partial reactors, where each partial reactor is assumed to be a continuous stirred tank reactor (CSTR). Due to the arrangement of the HRs and TCs in the reaction zone of the considered reactor, it is suitable to divide it into $N = 14$ partial reactors, as schematically shown in Figure 2. In this way, the rows of HRs are located in the centers of the partial reactors. Moreover, the rows of TCs are located at the boundaries of the partial reactors, which allows the determination of the reactor temperature in each partial reactor. In addition, the comparatively small number of CSTR elements simulates a deviation from the ideal plug flow tubular reactor as reported by Geißelbrecht et al. [12]. The discretized stationary conversion $\overline{X}_k$ at the end of the partial reactor k can be expressed by

$$\overline{X}_k \coloneqq \overline{X}(k\Delta z) \text{ for } k = 0, \ldots, N, \tag{20}$$

where Δz is the length in z-direction of a partial reactor. The conversion $\overline{X}_0$ at the beginning of the reactor is assumed to be zero, since the LOHC feed $\dot{V}_{\mathrm{LOHC,in}} = \dot{V}_{\mathrm{L},1}$ consists only of H18-DBT. The set of equations for describing the hydrogen volume flow $\overline{\dot{V}}_{\mathrm{H_2}}$ at steady-state operating points finally results in

$$0 = -u_{\mathrm{L},k} \frac{\overline{X}_k - \overline{X}_{k-1}}{\Delta z} + r_{\mathrm{X},k} \text{ for } k = 1, \ldots, N, \tag{21a}$$

$$\overline{\dot{V}}_{\mathrm{H_2}} = 9 \frac{c_{\mathrm{H18-DBT}}}{c_{\mathrm{H_2,N}}} \dot{V}_{\mathrm{L},N} \overline{X}_N, \tag{21b}$$

where $u_{\mathrm{L},k} \coloneqq u_\mathrm{L}(\dot{V}_{\mathrm{L},k}, T, p, \overline{X}_k)$ is the flow velocity of partial reactor k and $r_{\mathrm{X},k} \coloneqq r_\mathrm{X}(T, p, \overline{X}_k)$ is the reaction rate of partial reactor k.

In the following, the function for calculating the conversion in the last partial reactor is

$$\overline{X}_N =: f_{\overline{X}_N}(\boldsymbol{z}) \text{ s.t. } (21), \tag{22}$$

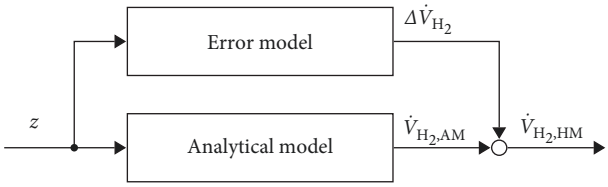

FIGURE 3: Structure of the hybrid model with parallel approach [19]. AM, analytical model; HM, hybrid model.

and for calculating the hydrogen volume flow

$$\overline{\dot{V}}_{H_2} =: f_{\dot{V}_{H_2}}(\boldsymbol{z}) \text{ s.t. } (21), \tag{23}$$

with the input vector $\boldsymbol{z}$ defined in Equation (1). Note that the subordinate solution of the set of Equations (21a) and (21b) in the functions is assumed.

3.5. Hybrid Model. In the previous section, some effects were neglected in the modeling and simplifications were made, such as neglection of dispersion, the simplified reaction kinetics or assumption of equal flow velocity, since a mathematical description is not possible or no data are available. To improve the obtained AM and to take these effects and simplifications into account, it is extended to a HM in the following. This approach is often used for chemical processes and contributes significantly to model improvement, as will be shown in Section 4.

Sohlberg and Jacobsen [19] have presented and compared different methods of gray box modeling. For the present problem, a HM with a parallel approach is suitable as shown in Figure 3. Here, the output signal of the black box model is added to the output signal of the AM. The resulting signal is finally the output of the HM. In a sense, the black box model reproduces the error of the AM, which is why it is called an additive error model in the following. Applying the introduced model structure of the HM results in

$$f_{\dot{V}_{H_2,HM}}(\boldsymbol{z}) = f_{\dot{V}_{H_2,AM}}(\boldsymbol{z}) + f_{\Delta\dot{V}_{H_2}}(\boldsymbol{z}), \tag{24}$$

where $f_{\dot{V}_{H_2,HM}}(\boldsymbol{z})$ is the function of the HM, $f_{\dot{V}_{H_2,AM}}(\boldsymbol{z})$ is the function of the AM (Equation 23), and $f_{\Delta\dot{V}_{H_2}}(\boldsymbol{z})$ is the function of the error model of the hydrogen volume flow rate. The conversion $\overline{X}_{N,HM}$ of the HM can be calculated from the hydrogen volume flow of the HM by

$$\overline{X}_{N,HM} = \frac{c_{H_2,N}}{9c_{H18-DBT,in}\dot{V}_L}\dot{V}_{H_2,HM} =: f_{\overline{X}_N,HM}(\boldsymbol{z}). \tag{25}$$

A purely data-based approach for the black box error model is GPR. A Gaussian process (GP) is a nonparametric stochastic model that is completely described by its mean function $m(\boldsymbol{z})$ and its covariance function $k(\boldsymbol{z}_m, \boldsymbol{z}_n)$ [44]. Assuming that the GP represents a function $f(\boldsymbol{z})$, it is written as

$$f(\boldsymbol{z}) \sim \mathcal{GP}(m(\boldsymbol{z}), k(\boldsymbol{z}, \boldsymbol{z}')). \tag{26}$$

In GPR, the function $f(\boldsymbol{z})$ is directly mapped by prior in form of the data set with input $\boldsymbol{Z}$ and output $\boldsymbol{y}$. For the prediction of the test output y of a test input $\boldsymbol{z}$, the joint normal distribution $\mathcal{N}(\cdot)$ of the training output $\boldsymbol{y}$ and the test output y results in

$$\begin{bmatrix} \boldsymbol{y} \\ y \end{bmatrix} \sim \mathcal{N}\left(m(\boldsymbol{z}), \begin{bmatrix} k(\boldsymbol{Z},\boldsymbol{Z}) & k(\boldsymbol{Z},\boldsymbol{z}) \\ k(\boldsymbol{z},\boldsymbol{Z}) & k(\boldsymbol{z},\boldsymbol{z}) \end{bmatrix} \right). \tag{27}$$

The mean function $m(\boldsymbol{z})$ is often chosen to be zero. Alternatively, a constant or a polynomial can be fitted to the prior to represent a data drift. The most commonly used covariance function is the squared exponential kernel

$$k(\boldsymbol{z}_m, \boldsymbol{z}_n) = \sigma_F^2 \exp\left(\frac{\|\boldsymbol{z}_m - \boldsymbol{z}_n\|_2^2}{2l^2}\right) + \sigma_N^2 \delta_{m,n}, \tag{28}$$

where $\|\cdot\|_2$ is the Euclidean norm, σ_F^2 is the signal variance, σ_N^2 is the measurement noise variance, l is the length-scale parameter, and $\delta_{m,n}$ is the Kronecker delta. To predict the test output y for the test input $\boldsymbol{z}$, the conditional distribution leads to the posterior mean and variance functions

$$\mathrm{E}(\boldsymbol{z}) = m(\boldsymbol{z}) + k(\boldsymbol{z},\boldsymbol{Z})(k(\boldsymbol{Z},\boldsymbol{Z}))^{-1}(\boldsymbol{y} - m(\boldsymbol{Z})), \tag{29a}$$

$$\mathrm{Var}(\boldsymbol{z}) = k(\boldsymbol{z},\boldsymbol{z}) - k(\boldsymbol{z},\boldsymbol{Z})(k(\boldsymbol{Z},\boldsymbol{Z}))^{-1}k(\boldsymbol{Z},\boldsymbol{z}). \tag{29b}$$

The posterior mean $\mathrm{E}(\boldsymbol{z})$ and variance $\mathrm{Var}(\boldsymbol{z})$ describe the prediction and uncertainty of the model at the arbitrary test point $\boldsymbol{z}$. The signal variance σ_F^2, the measurement noise variance σ_N^2, and the length-scale parameter l are free parameters and generally called hyperparameters $\theta = [l, \sigma_F, \sigma_N]^T$. The most commonly used method to determine the hyperparameters is the minimization of the log marginal likelihood function

$$\min_\theta \log p(\boldsymbol{y}|\boldsymbol{Z},\theta) = -\frac{1}{2}\boldsymbol{y}^T k(\boldsymbol{Z},\boldsymbol{Z})^{-1}\boldsymbol{y} - \frac{1}{2}\log|k(\boldsymbol{Z},\boldsymbol{Z})| - \frac{n}{2}\log(2\pi), \tag{30}$$

where n is the number of data points in the data set [44].

4. Validation

The HM in the last section consists of an analytical and a data-driven part. The unknown coefficients of the AM have to be determined using measurement data from the presented reactor. The data-based error model consisting of a GP must also be trained with measured data. This section presents the parameterization and training of the models and the resulting model validation.

4.1. Parameterization of Analytical Model. The five unknown coefficients in the AM (Equations 21a and 21b) are the

TABLE 2: Determined dimensionless coefficients of the reaction kinetic (Equation 8) and the liquid holdup (Equation 5) as part of the analytical model.

a_{cat}	0.24229
$\overline{\alpha}$	0.09851
$\overline{\beta}$	0.53598
$\overline{\gamma}$	− 0.72823
$\overline{\delta}$	0.26710

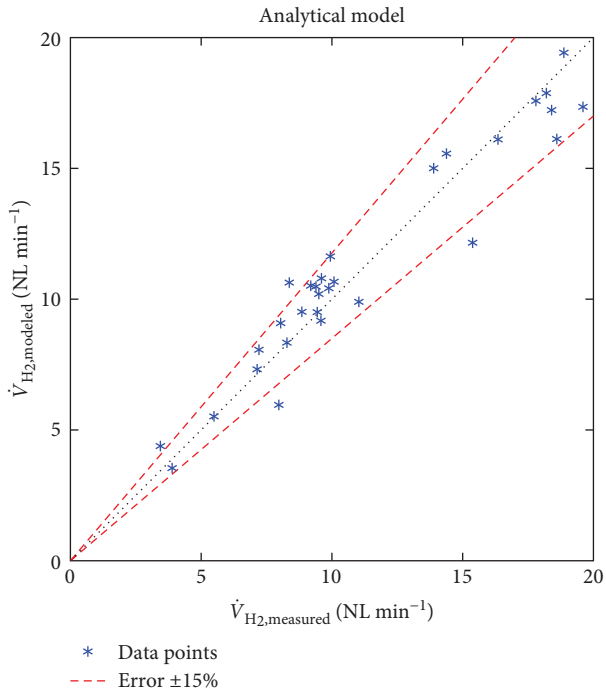

FIGURE 4: Comparison between the measured hydrogen volume flow $\dot{V}_{H_2,measured}$ and the hydrogen volume flow $\dot{V}_{H_2,modeled}$ calculated with the AM. AM, analytical model.

catalyst activity a_{cat} in the reaction kinetic (Equation 8) and the constants in the liquid holdup correlation (Equation 5), that is, $\overline{\alpha}, \overline{\beta}, \overline{\gamma}$, and $\overline{\delta}$. These are determined using a nonlinear least square regression analysis using 13 out of 30 available data points to parameterize a model that is as general as possible. The data points result from the best possible mapping of the value range of the reactor from the available data. The remaining 17 data points are used for validation.

The parameterized coefficients of the AM are shown in Table 2. The determined catalyst activity a_{cat} is quite small with 24.229%. This could result from the influence of simplifications made in the modeling. Note that the constants from the liquid holdup correlation differ from the results obtained in Stiegel and Shah [34] due to the different reactor setup, flow conditions, volume flows, and physical properties of the reactants.

A comparison of the measured and modeled hydrogen volume flow $\dot{V}_{H_2}$ using the AM with the determined parameters is shown in Figure 4. As can be seen, the fitted AM describes the behavior of the hydrogen volume flow in a qualitative manner. However, an error greater than 15% occurs at some data points. In addition, Table 3 shows the squared norm of the residual and the root mean square error (RMSE) of the parametrized AM.

TABLE 3: The squared norm of the residual and RMSE of the AM and HM.

	AM	HM
Residual (NL^2 min^{-2})	48.431	11.111
RMSE (NL min^{-1})	1.271	0.609

Abbreviations: AM, analytical model; HM, hybrid model; RMSE, root mean square error.

4.2. Training of Error Model. The training data set for the GP-based error model consists of the input vector of the reactor $\boldsymbol{z}$ and of the deviations of hydrogen volume flow $\dot{V}_{H_2}$ corresponding to

$$\Delta\dot{V}_{H_2} = \dot{V}_{H_2,measured} - \dot{V}_{H_2,AM} \tag{31}$$

between measurements and the output of the AM. A total of 20 data points are used for the training, consisting of the data points already used in the parameterization and seven additional data points. The remaining 10 data points are used to validate the training. For the GPR a squared exponential kernel is used. The hyperparameters were optimized to $l = 0.2038$, $\sigma_F = 1.2677$, and $\sigma_N = 0.3875$ by the training.

A comparison of the measured and modeled hydrogen volume flow $\dot{V}_{H_2}$ using the HM is shown in Figure 5. The deviations of the measured and modeled hydrogen flow rates are less than 15%. The majority of the data points even show a much smaller deviation. Compared to the deviations of the AM as shown in Figure 4, a significant improvement in model accuracy is visible. This improvement is also evident by comparing the residual and the RMSE of the two models, as shown in Table 3. Overall, the HM can describe the hydrogen volume flow rate with sufficient accuracy.

5. Optimization of Operating Points

In this section, the optimization of the operating points of the LOHC DH reactor is presented. For this purpose, first, the requirements for the operating points are defined and subsequently a corresponding optimization problem is formulated. Afterward, BO is presented as a method to solve the optimization problem and additionally, an approach for the global optimization of the acquisition function is applied as part of the BO.

5.1. Optimization Problem. As already described in Section 1, the energy required for endothermic DH is supplied in the form of heat. However, DH of LOHC can take place where no peripheral energy, such as waste heat from other processes, is available. Therefore, it has to be expensively produced from the released hydrogen, for example, by using a hydrogen burner [13]. For this reason, it is particularly important to utilize the LOHC to the best possible extent

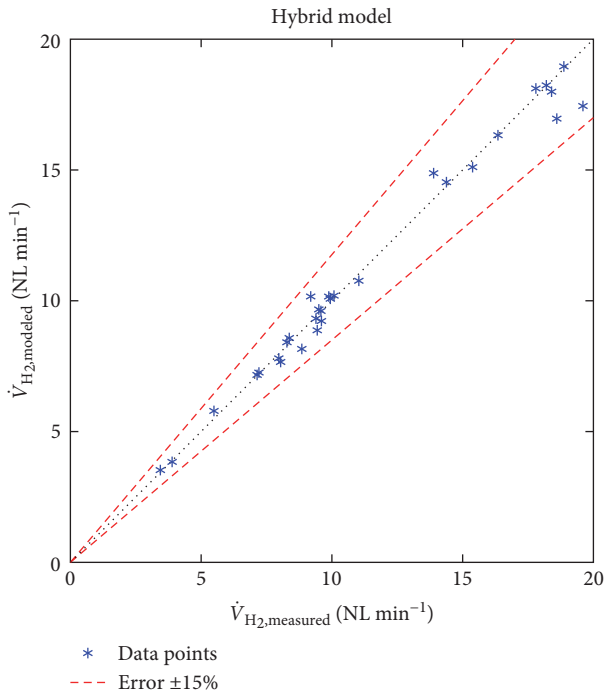

FIGURE 5: Comparison between the measured hydrogen volume flow $\dot{V}_{H_2,measured}$ and the hydrogen volume flow $\dot{V}_{H_2,modeled}$ calculated with the HM. HM, hybrid model.

and to keep the reactor temperature as low as possible, as this facilitates heat transfer. This can be achieved by a proper choice of the input variables (Equation 1) of the reactor for steady-state operating points.

Depending on the further use of the released hydrogen, there are certain requirements for an optimal operating point, which are explained below. Usually, downstream apparatuses for hydrogen purification and reconversion of hydrogen require a certain constant hydrogen volume flow $\dot{V}^*_{H_2}$, which has to be provided by the LOHC DH reactor or by a compressor, which reduces the efficiency of the complete process. Furthermore, these apparatuses are usually operated at a certain pressure. It is advantageous to operate the DH reactor at the same pressure p^* in order to avoid a subsequent compression and thus additional energy expenditures. The hydrogen yield from the LOHC can be expressed by the conversion at the end of the reactor $\overline{X}_N$. In the best case, this should be $\overline{X}^*_N = 1$ in order to utilize the LOHC in the best possible way. As already described, the reactor temperature should be as low as possible so that minimal released hydrogen has to be used to generate the required heat energy. This leads to $T^* = T^-$, which is the lower permissible reactor temperature. At last, the LOHC volume flow at the inlet of the reactor can be chosen freely.

From the listed requirements, a cost function $J(\boldsymbol{z})$ can be formulated which penalizes the deviations from the desired values quadratically. Due to the partly conflicting optimization goals, the requirements in $J(\boldsymbol{z})$ are prioritized by weights. In addition to the above optimization requirements, constraints on the input variables of the presented cuboid flow reactor have already defined in Equation (2). Overall, the following optimization problem is formulated as

$$\min_{\boldsymbol{z}\in\mathbb{R}^3} \quad J(\boldsymbol{z}) = \overline{q}_T(z_2 - T^-)^2 + \overline{q}_p(z_3 - p^*)^2 + \overline{q}_X\left(\overline{X}_N - 1\right)^2 + \overline{q}_{\dot{V}}\left(\dot{V}_{H_2} - \dot{V}^*_{H_2}\right)^2 \tag{32a}$$

$$\text{s.t.} \quad \boldsymbol{z}^- \le \boldsymbol{z} \le \boldsymbol{z}^+, \overline{X}_N = f_{\overline{X}_N}(\boldsymbol{z}) \;\&\; \dot{V}_{H_2} = f_{\dot{V}_{H_2}}(\boldsymbol{z}). \tag{32b}$$

The hierarchy of requirements is realized by a suitable empirical choice of the weights q_T, q_p, q_X, and $q_{\dot{V}}$, which serve as design parameters. To avoid numerical problems, the states are normalized to the range from 0 to 1, which is taken into account in the scaled weights $\overline{q}_T, \overline{q}_p, \overline{q}_X$, and $\overline{q}_{\dot{V}}$. The values of $\overline{X}_N$ and $\dot{V}_{H_2}$ can either be calculated by the presented HM (Equations 24 and 25) or measured at a DH reactor. The second option is very time consuming, so the number of observations that are required in the optimization should be kept as small as possible. Approaches such as BO are particularly suitable for this type of optimization problem.

5.2. Bayesian Optimization. BO is a powerful framework to find the extremum of a function whose mathematical description is unknown, nonconvex, or expensive to evaluate [23]. It is a sequential model-based approach that uses prior knowledge of the objective function $J(\boldsymbol{z})$ to sequentially update the model by adding more data points to find the extremum of the objective function [45]. The two main ingredients of the algorithm are the probabilistic surrogate model and the acquisition function.

The surrogate model uses the prior distribution and represents the objective function with its probabilistic uncertainty. As a result, the complete available knowledge is used to present the process. The surrogate model $J(\boldsymbol{z})$ is often represented by a GP, which, in addition to the expected value, specifies the uncertainty in form of the variance at the analyzed point:

$$J(\boldsymbol{z}) \sim \mathcal{GP}(m(\boldsymbol{z}), k(\boldsymbol{z}, \boldsymbol{z}')|\mathcal{D}_i). \tag{33}$$

Thereby, $\mathcal{D}_i$ is the data set in iteration i of the BO that was used to train the GP. The GP has already been described in Section 3.5.

There are a large number of acquisition functions that have different features and benefits. A good overview of the different functions is given by Brochu, Cora, and De Freitas

[23] and Shahriari et al. [45]. A common acquisition function is the expected improvement (EI)

$$EI(\boldsymbol{z}|\mathscr{D}_i) = \mathrm{E}\big(\max\{J_{\min,i} - J(\boldsymbol{z}), 0\}\big), \tag{34}$$

where $J_{\min,i} = \min\{J_1, \ldots, J_i\}$ [46]. The EI balances the trade-off between the exploration of unknown areas (global search) and the exploitation of known areas (local optimization) [23]. For Gaussian variables, as they are assumed here, the analytical closed form is given by

$$\begin{aligned} EI(\boldsymbol{z}|\mathscr{D}_i) = \big(J_{\min,i} - \mathrm{E}(\boldsymbol{z}|\mathscr{D}_i)\big)\Phi\left(\frac{J_{\min,i} - \mathrm{E}(\boldsymbol{z}|\mathscr{D}_i)}{\sqrt{\mathrm{Var}(\boldsymbol{z}|\mathscr{D}_i)}}\right) \\ + \mathrm{Var}(\boldsymbol{z}|\mathscr{D}_i)\phi\left(\frac{J_{\min,i} - \mathrm{E}(\boldsymbol{z}|\mathscr{D}_i)}{\sqrt{\mathrm{Var}(\boldsymbol{z}|\mathscr{D}_i)}}\right) \end{aligned} \tag{35}$$

with the normal cumulative distribution function $\Phi(\cdot)$ and the probability density function $\phi(\cdot)$. To maximize the EI, the acquisition function a is defined by

$$a(\boldsymbol{z}|\mathscr{D}_i) = -EI(\boldsymbol{z}|\mathscr{D}_i). \tag{36}$$

This specifies the utility of the posterior model that results from evaluating the objective function at the analyzed point. To find the extremum of the objective function $J(\boldsymbol{z})$, the acquisition function a is optimized iteratively, considering potential equality and inequality constraints $g(\boldsymbol{z}) = 0$ and $h(\boldsymbol{z}) \leq 0$. In the case of the considered LOHC DH reactor, only inequality constraints resulting from the physical box constraints (Equation 2) are existent. Subsequently, in each iteration i, the objective function is evaluated at the determined optimal point and the surrogate model is updated in terms of the GP. The sequential procedure is executed $i_{\max}$ iterations until a termination criterion is fulfilled. Finally, the optimal solution $(\boldsymbol{z}_{\mathrm{opt}}, J(\boldsymbol{z}_{\mathrm{opt}}))$ at iteration i_{opt} is returned. The sequence of BO for optimization of steady-state operating points is shown in Algorithm 1.

5.3. Global Optimization of Acquisition Function. BO requires the global minimum of the optimization problem (Equations 37a and 37b). Since the acquisition function (Equation 36) is usually a nonconvex function, a conventional gradient-based approach typically does not converge to the global optimum. Androulakis, Maranas, and Floudas [47] presented an algorithm called αBB, which is a method for global optimization of constrained nonconvex problems.

The basic idea of the algorithm is to convexify nonconvex terms by overpowering the nonconvexity of the origin term with the addition of convex quadratic functions in $\boldsymbol{z}$. Thus, the convexified acquisition function a_{conv} is given by

1: Initial data set: $\mathscr{D}_0 = (\mathbf{Z}_0, J(\mathbf{Z}_0))$
2: Train GP with $\mathscr{D}_0$:

$$J(\boldsymbol{z}) \sim \mathscr{GP}(m(\boldsymbol{z}),\, k(\boldsymbol{z}, \boldsymbol{z}')|D_0)$$

3: for $i \leftarrow i_0$ to $i_{\max}$ **Do**
4: Minimize acquisition function a over GP:

$$\boldsymbol{z}_i = \arg\min_{\boldsymbol{z}} \; a(z|\mathscr{D}_{i-1}) \tag{37a}$$

$$\text{s.t.} \quad g(\mathbf{z}) = 0,\, \mathrm{h}(\mathbf{z}) \leq 0 \tag{37b}$$

5: Evaluate process at $\boldsymbol{z}_i$ and expand data set:

$$\mathscr{D}_i = \{\mathscr{D}_{i-1},\, (\boldsymbol{z}_i,\, J(\boldsymbol{z}_i))\}$$

6: Train GP with $\mathscr{D}_i$:

$$J(\boldsymbol{z}) \sim \mathscr{GP}(m(\boldsymbol{z}),\, k(\boldsymbol{z}, \boldsymbol{z}')|D_i)$$

7: End for
8: Return optimal solution: $(\boldsymbol{z}_{\mathrm{opt}}, J(\boldsymbol{z}_{\mathrm{opt}}))$ at $i = i_{\mathrm{opt}}$

Algorithm 1: Bayesian optimization.

$$a_{\mathrm{conv}}(\boldsymbol{z}) = a(\boldsymbol{z}) + \sum_{j=1}^{3} \alpha_j(\boldsymbol{z}^-, \boldsymbol{z}^+)\left(z_j^- - z_j\right)\left(z_j^+ - z_j\right), \tag{38}$$

with the lower and upper bound $\boldsymbol{z}^{\pm} = [z_1^{\pm}, z_2^{\pm}, z_3^{\pm}]^{\mathrm{T}}$ of the input vector $\boldsymbol{z}$ and the nonnegative coefficients

$$\alpha_j(\boldsymbol{z}^-, \boldsymbol{z}^+) \geq \max\left\{0, -\frac{1}{2}\min_{\boldsymbol{z}^- \leq \boldsymbol{z} \leq \boldsymbol{z}^+} \lambda(\boldsymbol{z})\right\}, \tag{39}$$

where $\lambda(\boldsymbol{z})$ are the eigenvalues of the Hessian matrix of a_{conv} over $z_j^- \leq z_j \leq z_j^+$, $j \in 1, 2, 3$. In Maranas and Floudas [48], the eigenvalues of the Hessian matrix are calculated using the concept of the measure of a matrix. Further information about the algorithm can be found in Androulakis, Maranas, and Floudas [47].

6. Evaluation of Operating Point Optimization

In order to evaluate the optimization of operating points, the application scenario and the resulting optimization requirements are explained below. Afterward, the optimization concepts are presented before finally the results are given and the optimization concepts are compared with each other.

6.1. Optimization Scenario. It is assumed that the hydrogen produced by the LOHC DH reactor is subsequently used in a proton exchange membrane fuel cell (PEMFC). In order to achieve a desired output of the PEMFC, a certain hydrogen volume flow rate is required. In this evaluation, hydrogen volume flow rates $\dot{V}_{\mathrm{H_2}}^*$ of 10 NL min^{-1} and 18 NL min^{-1} are

Table 4: Desired optimization variables and scaled/unscaled weights for the optimization scenario.

T^*	280°C	q_T	20	$\overline{q}_T$	0.0125 K^{-2}
p^*	2 bar(a)	q_p	500	$\overline{q}_p$	125 $bar(a)^{-2}$
$\overline{X}_N^*$	1	q_X	200	$\overline{q}_X$	200
$\dot{V}_{H_2}^*$	(10, 18) NL min^{-1}	$q_{\dot{V}}$	2500	$\overline{q}_{\dot{V}}$	3.698 min^2NL^{-2}

Note: The variables marked with (*) are the desired optimization variables.

Table 5: Optimized steady-state operating points, cost functions, and optimization process metrics of the three considered optimization procedures, the model-based NO with HM, the model-based BO with HM, and the model-free BO with RMs, for $\dot{V}_{H_2}^* = 10$ NL min^{-1}.

	NO with HM	BO with HM	BO with RM
$\dot{V}_{LOHC,in}$ (Lh^{-1})	1.45	1.44	1.41
T (°C)	310.50	313.17	313.98
p (bar(a))	2.00	2.00	2.07
$\dot{V}_{H_2}$ (NL min^{-1})	9.87	9.95	10.08
$\overline{X}_N$	0.647	0.655	0.677
J_{min}	36.597	37.539	35.875
i_{max}	14	15	20
i_{opt}	13	13	11

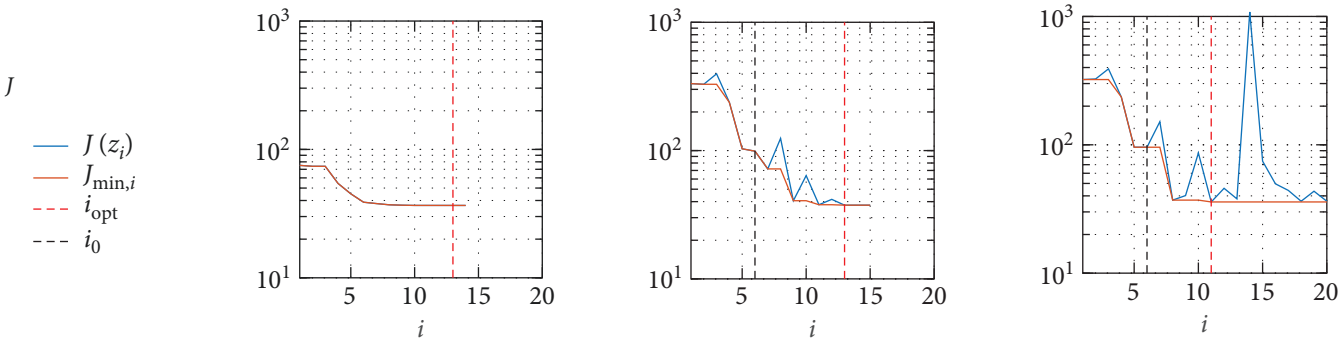

Abbreviations: BO, Bayesian optimization; HM, hybrid model; NO, nonlinear optimization; RMs, reactor measurements.

considered. The operating pressure of the PEMFC is assumed to be 2 bar(a), resulting in the desired value p^* for the reactor pressure. Since no process heat can be obtained from the PEMFC to operate the DH reactor, the reactor temperature should be as low as possible to enable integration with potential waste heat sources.

The constraints of the optimization variables described in the optimization problem (Equations 32a and 32b) result from the physical box constraints (Equation 2) of the reactor presented in Section 2, which is used for the evaluation. The desired values are shown in Table 4. Since the optimization objectives are partially conflicting, the requirements are prioritized accordingly. This is realized by an empirical choice of the weights q_T, q_p, q_X, and $q_{\dot{V}}$ of the normalized squared deviations of the optimization variables from the desired values, which was carried out using simulations according to the hierarchy of the requirements. The normalization of the states is taken into account in the scaled weights $\overline{q}_T$, $\overline{q}_p$, $\overline{q}_X$, and $\overline{q}_{\dot{V}}$, see Table 4.

In this evaluation, three optimization procedures are investigated and subsequently compared with each other. These are

- a model-based NO with HM,
- a model-based BO with HM, and
- a model-free BO with reactor measurements (RMs).

These three optimization procedures allow to evaluate the performance of BO in comparison to NO using the two model-based procedures with the HM. Moreover, they allow for a comparison of model-based and model-free BO. The algorithm used for the NO is SQP. This algorithm is also used as a solver for the global optimization of the acquisition function in the BO. In these cases of the model-based NO and BO, the presented and validated HM is used for the evaluation of the cost function $J(\boldsymbol{z})$, whereas in the case of model-free optimization, RMs are used to evaluate the cost function $J(\boldsymbol{z})$. To generate the initial data set $\mathcal{D}_0$ of the BO, $i_0 = 6$ data points are selected that are distributed over the entire value range, and the cost function $J(\boldsymbol{z})$ is evaluated accordingly.

6.2. Experimental Results. The results of the operating point optimization with the three procedures for the two considered hydrogen volume flow rates $\dot{V}_{H_2}^*$ of 10 NL min^{-1} and 18 NL min^{-1} are shown in Tables 5 and 6.

TABLE 6: Optimized steady-state operating points, cost functions, and optimization process metrics of the three considered optimization procedures, the model-based NO with HM, the model-based BO with HM, and the model-free BO with RMs, for $\dot{V}^*_{H_2} = 18\,\mathrm{NL\,min^{-1}}$.

	NO with HM	BO with HM	BO with RM
$\dot{V}_{\mathrm{LOHC,in}}$ ($\mathrm{Lh^{-1}}$)	2.61	2.63	2.64
T (°C)	320.00	320.00	319.76
p (bar(a))	2.00	2.00	2.02
$\dot{V}_{H_2}$ ($\mathrm{NL\,min^{-1}}$)	17.28	17.35	18.20
$\overline{X}_N$	0.628	0.625	0.653
$J_{\min}$	49.628	49.683	44.019
$i_{\max}$	9	13	12
i_{opt}	8	8	8

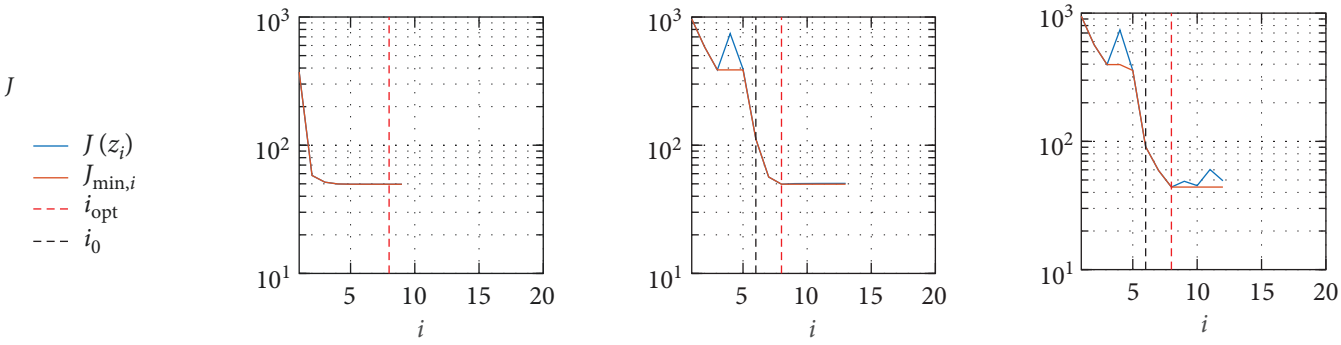

Abbreviations: BO, Bayesian optimization; HM, hybrid model; NO, nonlinear optimization; RMs, reactor measurements.

For the required hydrogen volume flow rate $\dot{V}^*_{H_2} = 10\,\mathrm{NL\,min^{-1}}$, all three optimization procedures find almost the same operating points. Compared to the optimized operating points of the two BO procedures, the reactor temperature T of the NO deviates slightly downward. However, it is well seen that despite the higher prioritized maximization of conversion $\overline{X}_N$, T was lowered enough to obtain the best possible tradeoff between hydrogen release and lowering the temperature for easier heat integration and more selective DH. The optimized reactor pressure p is at the lower limit of the value range. The desired hydrogen volume flow rate $\dot{V}^*_{H_2}$ is provided mostly reliably by all three optimization procedures and also the conversions $\overline{X}_N$ are in the range of 64%–68%. Only a small deviation is observed between the operating point optimization with the HM and with the RMs, suggesting sufficient accuracy of the HM in this range. As mentioned above, the conversion could be further increased by raising the reactor temperature, but this would mean to apply harsher process conditions with a potential production of unwanted heavy-boiling side-products (HBSPs). The HBSPs reduce the possible storage cycles of the LOHC material and can change the physical properties, which is not desired.

Table 5 also shows the curves of the cost function $J(\boldsymbol{z}_i)$ plotted over iterations i. It is seen that for all procedures, the minimum costs $J_{\min,i} = \min\{J_1, \ldots, J_i\}$ up to the respective iteration i decreases strongly in a few iterations. The high costs up to the initial iteration i_0 are caused by the initial data set $\mathscr{D}_0$. This is distributed over the entire value range of the reactor. The singular peaks of the cost function $J(\boldsymbol{z}_i)$ are due to the exploration behavior of the BO.

The number of iterations $i_{\max}$ used are very small for the model-based procedures with the HM. For the model-free BO with the RMs, slightly more iterations are performed. The iteration i_{opt} of the optimal solution is nearly the same for all procedures. In case of the optimization with the RMs, $i_{\max}$ represents the process evaluations.

The second case with the desired hydrogen volume flow rate $\dot{V}^*_{H_2} = 18\,\mathrm{NL\,min^{-1}}$ is presented in Table 6. All methods find nearly the same steady-state operating point. The reactor temperature T in this case is at the upper limit of the value range. The reactor pressure p is still at the lower limit of the value range. The small deviations in the hydrogen volume flow rates $\dot{V}_{H_2}$ and conversions $\overline{X}_N$ of the HM and the RMs show that the HM does not model this range as well as in the first case, but still with a sufficient accuracy.

The cost functions $J(\boldsymbol{z}_i)$ show lower explorations for the two procedures with BO than for $\dot{V}^*_{H_2} = 10\,\mathrm{NL\,min^{-1}}$ case. The deviations of $\dot{V}_{H_2}$ and $\overline{X}_N$ explain the higher minimum costs $J_{\min}$ of the two procedures with the HM compared to the BO with the RMs. The number of used iterations $i_{\max}$ and the iteration i_{opt} of the optimal solution are smaller for $\dot{V}^*_{H_2} = 18\,\mathrm{NL\,min^{-1}}$ than for $\dot{V}^*_{H_2} = 10\,\mathrm{NL\,min^{-1}}$.

Overall, all three procedures perform well in both cases, $\dot{V}^*_{H_2} = 10\,\mathrm{NL\,min^{-1}}$ and $\dot{V}^*_{H_2} = 18\,\mathrm{NL\,min^{-1}}$. The two model-based procedures, the NO and the BO with the HM, show almost no differences. By comparing the operating points found with the HM and the RMs, it is evident that inaccuracies are still present in the model, but it has sufficient accuracy for optimization. This is also shown in the validation in Section 4. The model-free optimization of operating points using the BO with the RMs achieves the best results. The optimized operating

points have the lowest minimum costs $J_{\min}$ compared to the operating points of the model-based procedures and the conversions $\overline{X}_N$ are also higher. It should be emphasized that this method does not use any process knowledge but only measurement data, which means that it can be applied to these complex processes without much effort. However, measuring the steady-state data points requires a lot of time due to the slow transient process.

7. Conclusion

In this paper, the optimization of operating points of a LOHC DH reactor is presented. For this purpose, an analytic model is derived and subsequently extended to a HM with an additive error model. In particular, phenomena such as evaporation of LOHC are included. For the parameterized and trained HM, validation shows that sufficient accuracy is achieved.

As an alternative approach to the NO method, BO is presented for the optimization of operation points. In the evaluation, it is demonstrated that BO provides comparable results to NO with HM, both in conjunction with HM and the RMs. It should be emphasized that the model-free BO with the RMs provides even better results in terms of higher conversions and lower minimal costs of the cost function compared to the model-based optimization procedures studied. Thus, it could be shown that BO is a suitable approach for this type of optimization. Especially, it offers the advantage that no complex modeling has to be performed, as it is needed for gradient-based optimization approaches. In addition, more complex optimization scenarios can be realized, for example, where the variable that is expensive to evaluate must be taken into account in the constraints. A corresponding approach to this is provided by Bergmann and Graichen [49].

The presented AM has the potential for improvement. Simplifications have been made due to insufficient knowledge of the phenomena, which should be further investigated. Model improvement is also desirable in terms of LOHC DH reactor control. In particular, a suitable dynamic HM needs to be derived for dynamic reactor control. Furthermore, the application of BO to another LOHC system such as benzyltoluene (H0-BT)/perhydro-benzyltoluene (H12-BT) is interesting as it seems to clearly outperform the H0-DBT/H18-DBT LOHC system [50].

Data Availability Statement

The data that support the findings of this study are available from the corresponding author upon reasonable request.

Conflicts of Interest

Peter Wasserscheid is a cofounder and minority shareholder of Hydrogenious LOHC Technologies GmbH, Erlangen, a company that has commercialized equipment for hydrogen storage using the LOHC technology.

Funding

The authors received no specific funding for this work.

Acknowledgments

The authors wish to thank Felix Gackstatter and Florian Ortner for their support in the realization of the experimental setup and the measurements.

References

[1] M. Niermann, S. Drünert, M. Kaltschmitt, and K. Bonhoff, "Liquid Organic Hydrogen Carriers (LO-HCs) – Techno-Economic Analysis of LOHCs in a Defined Process Chain," *Energy & Environmental Science* 12, no. 1 (2019): 290–307.

[2] P. T. Aakko-Saksa, C. Cook, J. Kiviaho, and T. Repo, "Liquid Organic Hydrogen Carriers for Trans-Portation and Storing of Renewable Energy—Review and Discussion," *Journal of Power Sources* 396 (2018): 803–823.

[3] P. C. Rao and M. Yoon, "Potential Liquid-Organic Hydrogen Carrier (LOHC) Systems: A Review on Recent Progress," *Energies* 13, no. 22 (2020): 6040.

[4] M. Eypasch, M. Schimpe, A. Kanwar, et al., "Model-Based Techno-Economic Evaluation of an Electricity Storage System Based on Liquid Organic Hydrogen Carriers," *Applied Energy* 185, no. 1 (2017): 320–330.

[5] N. Brückner, K. Obesser, A. Bösmann, et al., "Evaluation of Industrially Applied Heat-Transfer Fluids as Liquid Organic Hydrogen Carrier Systems," *ChemSusChem* 7, no. 1 (2014): 229–235.

[6] K. Müller, K. Stark, V. N. Emel'yanenko, et al., "Liquid Organic Hydrogen Carriers: Thermophysical and Thermochemical Studies of Benzyl- and Dibenzyl-Toluene Derivatives," *Industrial & Engineering Chemistry Research* 54, no. 32 (2015): 7967–7976.

[7] H. Jorschick, P. Preuster, S. Dürr, et al., "Hydrogen Storage Using a Hot Pressure Swing Reactor," *Energy & Environmental Science* 10 (2017): 1652–1659.

[8] A. Fikrt, R. Brehmer, V.-O. Milella, et al., "Dynamic Power Supply by Hydrogen Bound to a Liquid Organic Hydrogen Carrier," *Applied Energy* 194 (2017): 1–8.

[9] P. Modisha, P. Gqogqa, R. Garidzirai, C. N. M. Ouma, and D. Bessarabov, "Evaluation of Catalyst Activity for Release of Hydrogen From Liquid Organic Hydrogen Carriers," *International Journal of Hydrogen Energy* 44, no. 39 (2019): 21926–21935.

[10] S. Park, M. Naseem, and S. Lee, "Experimental Assessment of Perhydro-Dibenzyltoluene Dehydrogenation Reaction Kinetics in a Continuous Flow System for Stable Hydrogen Supply," *Materials* 14, no. 24 (2021): 7613.

[11] P. Preuster, Q. Fang, R. Peters, et al., "Solid Oxide Fuel Cell Operating on Liquid Organic Hydrogen Carrier-Based Hydrogen—Making Full Use of Heat Integration Potentials," *International Journal of Hydrogen Energy* 43, no. 3 (2018): 1758–1768.

[12] M. Geißelbrecht, R. Benker, A. Seidel, and P. Preuster, "Modeling of the Continuous Dehydrogenation of Perhydro-Dibenzyltoluene in a Cuboid Reactor," *Energy Technology* 12, no. 4 (2024): 2300813.

[13] J. Bollmann, K. Mitländer, D. Beck, et al., "Burner-Heated Dehydrogenation of a Liquid Organic Hydrogen Carrier (LOHC) System," *International Journal of Hydrogen Energy* 48, no. 77 (2023): 30039–30056.

[14] A. Wunsch, M. Mohr, and P. Pfeifer, "Intensified LOHC-Dehydrogenation Using Multi-Stage Microstructures and Pd-Based Membranes," *Membranes* 8, no. 4 (2018): 112.
[15] J. Kadar, F. Gackstatter, F. Ortner, et al., "Boosting Power Density of Hydrogen Release From Lohc Systems by an Inverted Fixed-Bed Reactor Design," *International Journal of Hydrogen Energy* 59 (2024): 1376–1387.
[16] R. Fletcher, *Practical Methods of Optimization* (John Wiley & Sons, 2000).
[17] J. Nocedal and S. Wright, *Numerical Optimization* (Springer, 2006).
[18] N. Asprion, R. Böttcher, R. Pack, et al., "Gray-Box Modeling for the Optimization of Chemical Processes," *Chemi.e. Ingenieur Technik* 91, no. 3 (2019): 305–313.
[19] B. Sohlberg and E. W. Jacobsen, "Grey Box Modelling—Branches and Experiences," *IFAC Proceedings Volumes* 41, no. 2 (2008): 11415–11420.
[20] E. J. Molga, "Neural Network Approach to Support Modelling of Chemical Reactors: Problems, Resolutions, Criteria of Application," *Chemical Engineering and Processing: Process Intensification* 42, no. 8-9 (2003): 675–695.
[21] Y. Zhang, L. Thangavelu, T. Z. Taban, et al., "Development of Hybrid Machine Learning Model for Simulation of Chemical Reactors in Water Treatment Applications: Absorption in Aminoacid," *Environmental Technology & Innovation* 27 (2022): 102417.
[22] A. Shokry, M. Pérez-Moya, M. Graells, and A. Espuña, "Data-Driven Dynamic Modeling of Batch Processes Having Different Initial Conditions and Missing Measurements," in *Computer Aided Chemical Engineering*, 40, (Elsevier, 2017): 433–438.
[23] E. Brochu, V. M. Cora, and N. De Freitas, "A Tutorial on Bayesian Optimization of Expensive Cost Functions, With Application to Active User Modeling and Hierarchical Reinforcement Learning," (2010).
[24] J. Mockus, "Application of Bayesian Approach to Numerical Methods of Global and Stochastic Optimization," *Journal of Global Optimization* 4, no. 4 (1994): 347–365.
[25] D. R. Jones, M. Schonlau, and W. J. Welch, "Efficient Global Optimization of Expensive Black-Box Functions," *Journal of Global Optimization* 13, no. 4 (1998): 455–492.
[26] S. Streltsov and P. Vakili, "A Non-Myopic Utility Function for Statistical Global Optimization Algorithms," *Journal of Global Optimization* 14, no. 3 (1999): 283–298.
[27] D. R. Jones, "A Taxonomy of Global Optimization Methods Based on Response Surface," *Journal of Global Optimization* 21, no. 4 (2001): 345–383.
[28] F. Häse, L. M. Roch, C. Kreisbeck, and A. Aspuru-Guzik, "Phoenics: A Bayesian Optimizer for Chemistry," *ACS Central Science* 4, no. 9 (2018): 1134–1145.
[29] K. Y. Nandiwale, T. Hart, A. F. Zahrt, et al., "Continuous Stirred-Tank Reactor Cascade Platform for Self-Optimization of Reactions Involving Solids," *Reaction Chemistry & Engineering Journal* 7, no. 6 (2022): 1315–1327.
[30] A. M. Schweidtmann, A. D. Clayton, N. Holmes, E. Bradford, R. A. Bourne, and A. A. Lapkin, "Machine Learning Meets Continuous Flow Chemistry: Automated Optimization Towards the Pareto Front of Multiple Objectives," *Chemical Engineering Journal* 352 (2018): 277–282.
[31] J. Stecher, L. Kiltz, and K. Graichen, "Semi-Infinite Programming Using Gaussian Process Regression for Robust Design Optimization," in *Proceedings of European Control Conference (ECC)* (2022): 52–59
[32] G. F. Froment, K. B. Bischoff, and J. De Wilde, *Chemical Reactor Analysis and Design* (Wiley, 2011).
[33] G. Emig and E. Klemm, *Chemische Reaktionstechnik* (Springer Vieweg, 2017).
[34] G. J. Stiegel and Y. T. Shah, "Backmixing and Liquid Holdup in a Gas-Liquid Cocurrent Upflow Packed Column," *Industrial & Engineering Chemistry Process Design and Development* 16, no. 1 (1977): 37–43.
[35] A. Wunsch, T. Berg, and P. Pfeifer, "Hydrogen Production from the LOHC Perhydro-Dibenzyltoluene and Purification Using a 5 µm PdAg-Membrane in a Coupled Microstructured System," *Materials* 13, no. 2 (2020): 277.
[36] T. Solymosi, M. Geißelbrecht, S. Mayer, et al., "Nucleation as a Rate-Determining Step in Catalytic Gas Generation Reactions From Liquid Phase Systems," *Science Advances* 8, no. 46 (2022): 3262.
[37] L. C. Grotz, "Heterogeneous Equilibria in General Chemistry," *Journal of Chemical Education* 40, no. 9 (1963): 479.
[38] S. Dürr, S. Zilm, M. Geißelbrecht, et al., "Experimental Determination of the Hydrogenation/Dehydrogenation—Equilibrium of the LOHC System H0/H18-Dibenzyltoluene," *International Journal of Hydrogen Energy* 46, no. 64 (2021): 32583–32594.
[39] A. Jess and P. Wasserscheid, *Chemical Technology* (Wiley-VCH, 2013).
[40] R. B. Bird, W. E. Stewart, and E. N. Lightfoot, "Transport Phenomena," (Wiley) (2007).
[41] D. W. Green and M. Z. Southard, *Perry's Chemical Engineers' Handbook* (McGraw-Hill Education, 2019).
[42] H. Jorschick, M. Geißelbrecht, M. Eßl, P. Preuster, A. Bösmann, and P. Wasserscheid, "Benzyltoluene/Dibenzyltoluene-Based Mixtures as Suitable Liquid Organic Hydrogen Carrier Systems for Low Temperature Applications," *International Journal of Hydrogen Energy* 45, no. 29 (2020): 14897–14906.
[43] J. M. Prausnitz and F. H. Shair, "A Thermodynamic Correlation of Gas Solubilities," *AIChE Journal* 7, no. 4 (1961): 682–687.
[44] C. E. Rasmussen, *Gaussian Processes for Machine Learning* (MIT Press, 2006).
[45] B. Shahriari, K. Swersky, Z. Wang, R. P. Adams, and N. de Freitas, "Taking the Human Out of the Loop: A Review of Bayesian Optimization," *Proceedings of the IEEE* 104, no. 1 (2016): 148–175.
[46] J. Mockus, V. Tiesis, and A. Zilinskas, "The Application of Bayesian Methods for Seeking the Extremum," in *Towards Global Optimization*, eds. L. C. W. Dixon and G. P. Szegö, 2, (North-Holland, 1978): 117–129.
[47] I. P. Androulakis, C. D. Maranas, and C. A. Floudas, "Floudas, αBB: A Global Optimization Method for General Constrained Nonconvex Problems," *Journal of Global Optimization* 7, no. 4 (1995): 337–363.
[48] C. D. Maranas and C. A. Floudas, "Global Minimum Potential Energy Conformations of Small Molecules," *Journal of Global Optimization* 4, no. 2 (1994): 135–170.
[49] D. Bergmann and K. Graichen, "Safe Bayesian Optimization Under Unknown Constraints," in *Proceedings of 59th IEEE Conference on Decision and Control (CDC)*, (IEEE, 2020): 3592–3597.
[50] T. Rüde, S. Dürr, P. Preuster, M. Wolf, and P. Wasserscheid, "Benzyltoluene/Perhydro Benzyltoluene—Pushing the Performance Limits of Pure Hydrocarbon Liquid Organic Hydrogen Carrier (LOHC) Systems," *Sustainable Energy & Fuels* 6, no. 6 (2022): 1541–1553.